Deactivation of highly excited CS_2 and SO_2 by rare gases

Alexander Chimbayo, Beatriz M. Toselli,[a] and John R. Barker[b]
Department of Chemistry and Department of Atmospheric, Oceanic and Space Sciences, The University of Michigan, Ann Arbor, Michigan 48109-2143

(Received 16 August 1996; accepted 30 October 1997)

The time dependent thermal lensing (TDTL) technique has been used to study collisional energy transfer from highly excited CS_2 in baths of Xe, Kr, and Ar, and from highly excited SO_2 in Kr and Ar. Bath gas pressures ranged from about 50 to about 600 Torr. The data were analyzed by simulating the observed TDTL signals with a unified hydrodynamic TDTL theory. The results are expressed in terms of $\langle \Delta E \rangle$, the bulk average energy transferred per collision as a function of $\langle E \rangle$, the mean energy content. The results show that $\langle \Delta E \rangle$ increases dramatically at $\langle E \rangle \approx 17\,500-23\,500\ \mathrm{cm}^{-1}$ for CS_2 deactivation, and at $\langle E \rangle \approx 18\,000-22\,500\ \mathrm{cm}^{-1}$ for SO_2 deactivation. This enhancement of energy transfer, which was observed previously in NO_2 and CS_2 deactivation, has been linked to the presence of nearby excited electronic states. Furthermore, at lower energy, our results reveal an unusual systematic dependence of $\langle \Delta E \rangle$ on bath pressure; energy transfer per collision is significantly more efficient at lower collision frequency. These results and data from the literature can be explained with a phenomenological model which includes collisional vibrational relaxation within each of two sets of vibronic levels, and collision-induced intersystem crossing (CIISC), which exhibits mixed order kinetics. © *1998 American Institute of Physics.* [S0021-9606(98)00306-7]

I. INTRODUCTION

At low vibrational energies, molecules have sparse densities of states and the individual transitions can be resolved easily. For this sparse density of states regime, energy transfer (ET) models based on the Landau–Teller and the SSH theories[1] give semiquantitative agreement with experimental data,[2,3] and higher order theories give quantitative agreement.[4,5] The transition from small to large molecule behavior is of great interest[6,7] and can best be characterized in terms of the increase in vibrational state densities. At higher vibrational energies, ET behavior is more complicated, not only because of the increased densities of states, but also because low lying electronic states may interact with the ground electronic state. In studies involving triatomics, sharp increases in ET rates have been observed at energies where excited electronic states can mix with the ground state.[8–11]

Only a few ET studies of triatomics have been carried out at moderate to high energies. These include ultraviolet absorption (UVA) studies on CS_2,[12] and SO_2,[13] time-dependent thermal lensing (TDTL) measurements using NO_2[8] and CS_2,[14] fluorescence decay studies in the visible on NO_2,[15–17] infrared fluorescence of NO_2,[18] and time-resolved Fourier transform infrared emission (TR-FTIRE) studies of highly excited NO_2,[9,10(b)] CS_2,[10(a)] and SO_2.[11] That NO_2, SO_2, and CS_2 have been selected for studies of triatomics is no accident, because the low-lying excited electronic states of these species are strongly mixed with the electronic ground state[19] and it has been assumed in the ET studies that optical pumping of these triatomics produces states with predominantly ground state character.

In the present work, we have used the TDTL technique to investigate ET involving CS_2 and SO_2 (a preliminary report on part of this study has been published[14]). An important strength of the TDTL technique is that it monitors only the translational energy changes in the heat bath and does not depend on the spectroscopic properties of the excited species. However, to avoid ambiguities in interpretation, only monatomic colliders can be used. As in the previous TDTL study of NO_2[8] and in agreement with recent experiments by Dai and co-workers on NO_2,[9,10(b)] CS_2,[10(a)] and SO_2,[11] the present results show that energy transfer is markedly enhanced near the origins of low-lying electronic states in both CS_2 and SO_2. In addition, the present results show that energy transfer on a per-collision basis is more efficient at low pressures than at high pressures, as if the excited molecules ''remember'' a previous collision. This unusual ''memory'' effect can be explained with a model which includes collision-induced intersystem crossing (CIISC) between two sets of vibronic levels and collisional vibrational relaxation within each set. According to the model, the ''memory'' effect is a result of the CIISC rate saturating with increasing pressure (i.e., becoming pressure independent).[20–22]

Observations of pressure saturation effects in CIISC have been reported previously in phosphorescence lifetime measurements and quantum yield studies involving the $^3B_1$ state of SO_2 by Strickler and Rudolph,[20] and by Su *et al.*[21] For instance, the physical electronic quenching rate exhibited a linear pressure dependence at low quencher pressures, but tended to level off at high pressures. These experiments support earlier predictions by Freed,[22,23] who developed a generalized theory of collision-induced intersystem crossing.

[a]Permanent address: Universidad Nacional de Cordoba, Sucursal 16, C.C. 61.5016, Cordoba, Argentina.
[b]Author to whom correspondence should be addressed.

 © 1998 American Institute of Physics

TABLE I. Excitation conditions.

Absorber gas	Bath gas	Excitation wavelength used(nm)	Absorption cross section[a] ($\sigma\times10^{20}$ cm^2 molecule^{-1})	Laser dye
CS_2	Xe, Kr	320.00	4.4	DCM II
	Ar	320.34	11.7	DCM II
SO_2	Kr	320.00	4.9	DCM II
	Ar	292.00	73.4	Coumarin 560

[a]Reference 42.

Strickler and Rudolph found that the rate of physical quenching of the $^3B_1$ state of SO_2 was well represented by the empirical expression

$$\text{rate}=\frac{k_q P_M}{1+\alpha k_q P_M}, \tag{1}$$

where k_q is the bimolecular quenching rate coefficient and P_M is the pressure of the quenching gas. The limiting (pressure-independent) rate, α^{-1}, was found to be about 1.3×10^6 s^{-1}, and did not depend on the identity of the quencher.[20] Strickler and Rudolph proposed two possible simpler mechanisms for collisional quenching which can lead to pressure saturation.[20] One is a theoretical treatment of radiationless transitions from the $^3B_1$ state to the ground state (which is similar to Freed's theory[22,23]), and the other is a kinetic scheme involving other nearby triplet states. In the intermediate pressure region, the two mechanisms predict similar pressure dependences, but the kinetic scheme appeared to fit experimental data somewhat better, and leads to Eq. (1).

CIISC is a very important feature of the kinetic model we have used to interpret our data. The lowest lying triplet states ($^3B_2$ in both SO_2 and CS_2) appear to play the critical role in effecting the apparent pressure dependence of energy transfer. In addition to the ''memory effect,'' our kinetic model explains the enhanced energy transfer at high levels of vibrational excitation observed in the TDTL experiments and it explains why this enhancement is not observed in the UVA studies.[12,13] Although our proposed model is plausible, the experiments are indirect and the model must be verified by more direct techniques in future experiments.

II. EXPERIMENT

The optical arrangement and detection system of the TDTL technique have been described in detail elsewhere[8,24,25] and only a brief outline will be given here. Ultraviolet light was generated with a frequency doubled tunable dye laser (Lumonics HyperDye 300; InRad Tracker-II frequency doubler) pumped by a XeCl rare gas excimer laser (Lumonics HyperEx 400, 8–12 ns pulse duration) operating at 25 Hz. The specific laser dyes, excitation wavelengths, and corresponding absorption cross-sections for CS_2 and SO_2 are listed in Table I. At the laser fluences typically used in the experiments, less than 0.5% of the absorbing species is excited. A Scientech absorbing calorimetric power meter was used to measure the energy of the dye laser beam at the exit window of the cell. Average laser power was measured just prior to and immediately after each run, and it remained constant to within 5%. Corrections were applied for absorption and reflection of the laser beam by the optical components. The optical set-up and the detection system are shown schematically in Fig. 1.

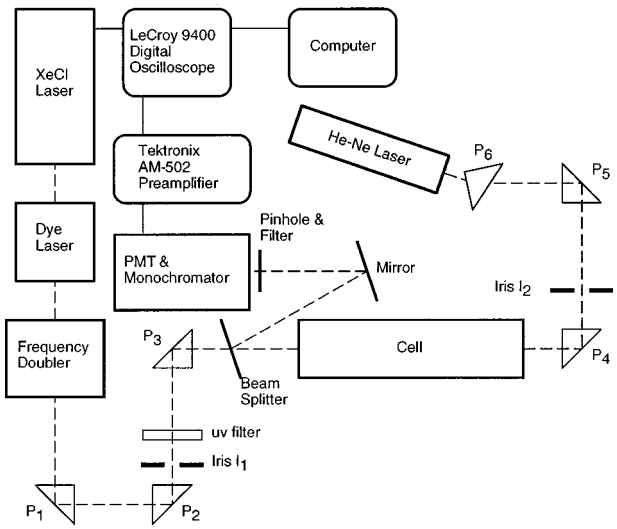

FIG. 1. A schematic of optical set-up and detection system used in the TDTL technique. Prisms are denoted as P_1, P_2, etc.

Energy from the excited species is transferred by collisions to the thermal bath, resulting in a small rise in temperature (typically <0.2 K). The consequent fluctuations in bath gas density and refractive index near the axis of the exciting laser beam produce a thermal lens. With time, this lens dissipates, largely due to thermal conductivity. The divergence of a low power CW He–Ne laser (Spectra-Physics 155A), counterpropagating coaxially with exciting laser, is used to monitor the time evolution of the thermal lens (note that prism P_6 prevents the pulsed laser light from entering the He–Ne laser cavity). The He–Ne laser beam divergence was observed by measuring the light transmitted through a pinhole situated at the center of the probe laser beam. This was accomplished with a photomultiplier tube (Hamamatsu PMT type 1P28), mounted at the exit slit of a 0.5 m Ebert monochromator which was fitted with a 623.8 nm interference filter and pinhole at the entrance slit. The response time of the PMT (with a 1200 Ω load resistor) was about 0.1 μs. The signal from the PMT was fed to a Tektronix AM 502 amplifier (bandpass from dc to 1 MHz) and averaged with a LeCroy 9400 digital oscilloscope for several thousand laser shots. The averaged signal was transferred to an Apple Macintosh computer for further analysis. For each run, signals were collected over the period 0–500 μs for use in the TDTL analysis and over longer times for determining the average radius of the exciting laser beam profile, as discussed below.

The digital oscilloscope was triggered with a timing pulse from the XeCl laser and there was a small time delay (~0.2 μs) between the timing pulse and the laser light pulse. Moreover, the response of the total electronic system to the timing pulse was not instantaneous, but persisted for a few microseconds. The instrumental response function

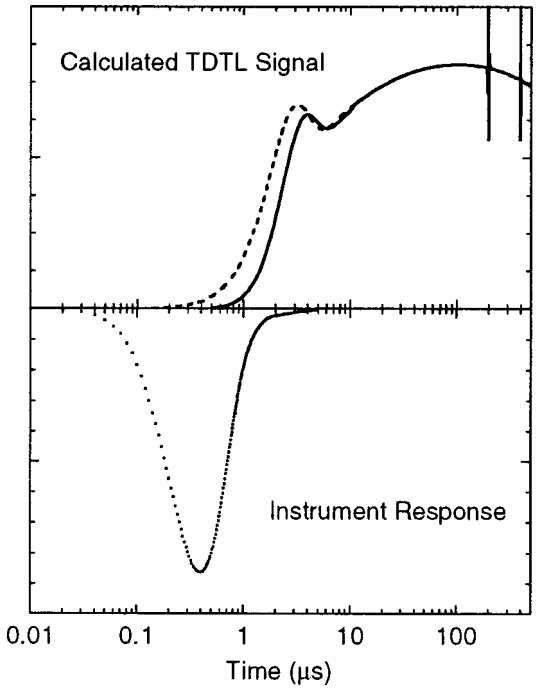

FIG. 2. A typical calculated TDTL signal, showing the effect of convolution with the electronic response signal (lower panel). The shape and duration of the response signals was always the same but the onset depends on the electronic settings.

shown in Fig. 2 was measured by observing a weak laser light pulse, which has a duration of only ~ 10 ns and is therefore essentially a delta function on the microsecond time scale of the experiments. In the analysis (see below), the instrument response function was numerically convolved with each simulated TDTL signal for comparison with the experimental TDTL signals.

The 89 cm long$\times$4.38 cm diameter Pyrex cell was fitted with Suprasil windows sealed with Viton O-rings. The cell was connected to a vacuum line and gas handling system at its midsection. A pair of capacitance manometers (MKS Baratron, model 227 for 0–1 Torr and model 122 for 0–1000 Torr) also were attached to the cell midsection. Prior to each set of runs, the cell was evacuated to less than 1 mTorr. The cell leak rate was less than 0.1 Torr/h and the duration of a typical run was 6–10 min. Contamination due to the air leaks is insignificant, because the leak rate is small, potential reactions are slow, and the collisional deactivation efficiencies of N_2 and O_2 are probably only slightly larger than those of the rare gases.

Based on the absorbed laser pulse energy and the heat capacity, we estimate that the maximum temperature change resulting from the lensing effect is less than 0.2 K. If photochemical reactions occur, they can produce additional small temperature changes and it is therefore essential that the systems under study be free of chemical reaction. There have been reports of CS_2 photodissociation at $\lambda > 308$ nm,[26–28] although the photodissociation threshold is at $\lambda = 272$ nm.[29] In all of these studies, large laser fluences were employed and multiphoton absorption was implicated. For SO_2, the photodissociation threshold wavelength is near 220 nm,[30] and evidence of photoproducts has appeared also only when multiphoton absorption is possible. In the present studies, multiphoton absorption and other potential photochemical complications were minimized by using low laser fluences and low partial pressures of CS_2 and SO_2.

The reagent CS_2 (Baker Reagents) and SO_2 (Matheson) were thoroughly degassed prior to use. Argon (Airco), Kr and Xe (Cryogenic Rare gases) of high nominal purity ($\geqslant 99.99\%$) were used without further purification.

III. THEORETICAL BACKGROUND

The analysis of TDTL signals has been described elsewhere in detail,[8,24,25,31] but it is useful to give a brief outline here. Following the excitation laser pulse, the initially excited molecules transfer energy to the heat bath. The temperature of the heat bath increases, causing a change in the index of refraction. Since the excitation laser beam is most intense at its center, the temperature rise is greatest near the beam center and the index of refraction change is greatest there. The divergence of a He–Ne laser is used to monitor the refractive index variations. Since the energy transfer can occur on a short time scale, the rapid density change can produce significant acoustic waves, which are accompanied by density and index of refraction fluctuations. The detailed behavior of the density near the beam center as a function of time is dominated first by the acoustic waves as they depart from near the beam center, and then by the continuing energy transfer process and finally by thermal conductivity, which dissipates the thermal lens. Diffusion of the excited species plays a lesser role, and viscosity plays such a small role that it can be neglected.[32]

A full analysis of the TDTL signal requires a fluid mechanics analysis which includes the spatial and temporal heat release (due to energy transfer), acoustic waves, thermal conductivity, and diffusion. In addition, the optics of the thermal lens must be considered. Flynn and co-workers[33] were the first to apply the TDTL technique to energy transfer studies. They developed a model for analysis of their results, but the model did not include thermal conductivity and diffusion, which were not very important in their experiments, but which are extremely important in most other experimental systems. An extension of their model was developed to include the missing factors and a key feature of the extended model is a zeroth-order Bessel function expansion, which was necessary to obtain a tractable solution.[24,31] This extended model has been tested by comparison with a full numerical treatment and it was pointed out that the use of the zeroth-order Bessel function expansion imposes incorrect radial boundary conditions, leading to a phase error in the calculated reflected acoustic waves.[32] Aside from this phase error, the two methods yield calculated signals that are virtually identical. Since the reflected acoustic waves play no role in the energy transfer data analysis, the phase error has no effect on the energy transfer results. The approximate model was used in the present study, as in the TDTL study of NO_2 energy transfer,[8] because it is sufficiently accurate and it is far more computationally efficient than the full numerical treatment.

The TDTL Signal, $S(t)$ is defined as

TABLE II. Physical constants (298 K) and Lennard-Jones parameters.[a]

	σ_{LJ} Å	ϵ/k K	Molar refractivity $cm^3\ mol^{-1}$	Heat capacity $cal\ K^{-1}\ mol^{-1}$	Thermal conductivity $10^5\ cal\ K^{-1}\ s^{-1}\ cm^{-1}$
CS_2	4.575	414.6	21.99[b]	10.85[e]	1.901[g]
SO_2	4.112	336.0	9.384[c]	9.529[e]	1.98[h]
Ar	3.542	93.3	4.143[d]	4.97[f]	4.165[i]
Kr	3.655	178.9	6.256[d]	4.97[f]	2.25[f]
Xe	4.047	231.0	10.155[d]	4.97[f]	1.30[f]

Collider pair	$10^{-7}\times k_{LJ}$ $Torr^{-1}\ s^{-1}$
CS_2–Xe	1.11
CS_2–Kr	1.04
CS_2–Ar	1.10
SO_2–Kr	0.91
SO_2–Ar	0.95

[a]L-J parameters for the rare gases are from Ref. 43, those for CS_2 are from Ref. 44, and those for SO_2 are from Ref. 45.
[b]Reference 46.
[c]Reference 47.
[d]Reference 48.
[e]Reference 43.
[f]Reference 49.
[g]Reference 50.
[h]Reference 51.

$$S(t)=1-I(t)/I_0, \tag{2}$$

where I_0 is the intensity (at beam center) of the He–Ne laser measured by the PMT before firing the excitation laser at $t=0$, and $I(t)$ is the corresponding intensity following the pulse.

A FORTRAN code, based on the extended TDTL theory[8,24,25,31] was formulated to calculate the TDTL signal, $S(t)$, using the physical constants in Tables I and II, and the experimental conditions listed in Tables III and IV. The rate coefficient, k_e, for the energy deposition entered the calculation as an empirical function of $\langle E\rangle$, the mean internal energy per molecule of the absorber. The functional form and parameters of k_e were adjusted by trial and error to reproduce, as accurately as possible, the shape and magnitude of the signals for each experiment. The signal magnitudes depend most strongly on bath gas molar refractivity, the absorber number density, the laser fluence, and the bath gas pressure. The *absolute* signal strengths calculated in the simulations generally agreed with the experiments within $\pm 30\%$. This level of agreement is very good, considering the experimental uncertainties in laser power and absorber concentration.

TABLE III. Experimental conditions and ET data: CS_2/rare gas systems.

Run #	Bath, M	M (Torr)	CS_2 (Torr)	E_{laser} (mJ)	F_{corr}[a]	r_b[b] (cm)	Parameters[c] of k_e 10^7A	a	E_c	B	b
1	Xe	50.0	0.005	0.28	1.32		0.10	2.00	4800	3.50	0.99
2		148.6	0.015	0.248	1.55		0.30	2.00	5500	4.25	1.03
3		302.0	0.030	0.292	1.49		0.60	1.80	6250	5.15	1.04
4		607.9	0.061	0.294	1.42	0.052	1.25	1.60	5500	6.75	1.02
5		50.8	0.005	0.237	1.26		0.11	2.00	4900	3.50	0.98
6		152.0	0.015	0.241	1.40		0.30	1.95	5500	4.20	1.02
7		302.0	0.031	0.238	1.50		0.60	1.70	5800	5.30	1.03
8		607.9	0.061	0.247	1.72	0.056	1.30	1.60	5500	6.25	1.00
9	Kr	50.8	0.021	0.136	1.00		0.07	1.80	4500	2.38	1.00
10		143.8	0.058	0.135	1.23		0.15	2.00	6000	3.00	1.00
11		300.0	0.122	0.135	1.24		0.30	1.80	6000	4.50	1.00
12		601.0	0.244	0.139	1.23	0.054	0.60	1.80	6000	5.00	1.00
13		49.2	0.019	0.119	1.13		0.06	2.20	4000	2.70	1.00
14		149.2	0.058	0.113	1.17		0.15	2.00	5500	3.80	1.00
15		296.9	0.115	0.120	1.12		0.33	1.80	5500	4.80	1.00
16		601.7	0.244	0.115	1.09	0.054	0.75	2.00	6400	5.75	1.00
17		52.3	0.021	0.113	1.00		0.06	1.60	4000	2.40	1.05
18		154.4	0.063	0.100	1.09		0.16	2.00	6000	3.80	1.00
19		299.9	0.121	0.219	1.62		0.30	1.80	6000	4.50	1.00
20		600.7	0.244	0.124	1.46	0.056	0.60	1.80	6000	5.00	1.00
21	Ar	50.4	0.011	0.222	1.75		0.10	1.80	4500	4.30	0.95
22		133.7	0.029	0.232	2.3		0.30	1.70	4000	5.25	1.00
23		303.1	0.066	0.234	2.25		0.64	1.75	5000	6.20	1.03
24		610.9	0.133	0.287	2.02	0.056	1.2	1.40	4500	7.00	1.00
25		50.3	0.011	0.196	1.7		0.09	1.75	4000	4.25	0.90
26		143.7	0.032	0.203	3.05		0.39	1.65	4000	5.25	0.98
27		302.0	0.067	0.205	3.30		0.60	1.65	5000	6.20	1.00
28		612.9	0.136	0.209	2.45	0.058	1.20	1.40	5000	7.00	1.00

[a]Magnitude of simulated signal scaled by factor, F_{corr}. For most runs, the magnitude of simulations were within 30% of those of experiment.
[b]Value determined at the highest pressure in a set of runs is used in simulations for all pressures.
[c]$k_e=A\ \exp((E_0-\langle E\rangle)/(E_c))^a+B\langle E\rangle^b$, where A, a, E_c, B, and b are empirical parameters, E_0 is the initial excitation energy, k_e is in units of $cm^3\ s^{-1}$.

TABLE IV. Experimental conditions and ET data: SO_2/rare gas systems.

Run #	Bath, M	M (Torr)	SO_2 (Torr)	E_{laser} (mJ)	F_{corr}[a]	r_b[b] (cm)	Parameters[c] of k_e				
							10^7A	a	E_c	B	b
1	Kr	75.5	0.031	0.070	0.82		0.07	1.80	4500	2.38	1.00
2		148.0	0.061	0.072	0.71		0.15	2.00	6000	3.00	1.00
3		299.8	0.124	0.075	0.87		0.30	1.80	6000	4.50	1.00
4		611.2	0.252	0.084	0.60	0.064	0.60	1.80	6000	5.00	1.00
5		73.7	0.030	0.126	0.65		0.06	2.20	4000	2.70	1.00
6		151.4	0.062	0.123	0.73		0.15	2.00	5500	3.80	1.00
7		304.1	0.127	0.127	0.77		0.33	1.80	5500	4.80	1.00
8		607.9	0.248	0.112	0.58	0.071	0.75	2.00	6400	5.75	1.00
9		73.4	0.031	0.089	0.80		0.06	1.60	4000	2.40	1.05
10		154.2	0.064	0.098	0.86		0.16	2.00	6000	3.80	1.00
11		309.7	0.129	0.107	0.90		0.30	1.80	6000	4.50	1.00
12		626.5	0.260	0.105	0.78	0.064	0.60	1.80	6000	5.00	1.00
13	Ar	112.0	0.042	0.05	1.65		0.20	1.55	5000	5.00	1.00
14		303.9	0.125	0.05	0.90		0.60	1.50	6000	6.75	1.00
15		603.0	0.244	0.05	0.71	0.065	1.00	1.55	6000	7.50	0.98
16		114.5	0.046	0.05	1.40		0.20	1.65	5300	4.50	0.99
17		306.0	0.124	0.05	0.94		0.50	1.55	5000	6.20	0.98
18		610.0	0.251	0.05	2.05	0.071	1.00	1.55	6000	7.80	0.99
19		114.5	0.046	0.05	1.60		0.20	1.65	5300	4.50	0.99
20		282.0	0.119	0.05	1.69		0.58	1.55	6000	6.75	1.00
21		606.0	0.251	0.05	1.23	0.069	1.20	1.55	6000	7.80	1.02

[a]Magnitude of simulated signal scaled by factor, F_{corr}. For most runs, the magnitude of simulations were within 30% of those of experiment.
[b]Value determined at the highest pressure in a set of runs is used in simulations for all pressures.
[c]$k_e = A\ \exp((E_0 - \langle E\rangle)/(E_c))^a + B\langle E\rangle^b$, where A, a, E_c, B, and b are empirical parameters, E_0 is the initial excitation energy, k_e is in units of $cm^3\ s^{-1}$.

IV. RESULTS

A. Analysis of experimental TDTL signals

Figure 3 shows typical experiment TDTL signals obtained from dilute mixtures ($<1/2500$) of CS_2 in Ar, Kr, and Xe bath gases at ~ 600 Torr. The relative signal amplitudes depend mostly on the molar refractivities (see Table II). An initial fast transient spike is observed in all signals because rapid energy deposition at early times produces interference among the departing acoustic waves.[8,24] The fast transients appearing at $\sim 273\ \mu s$ for Ar and at $\sim 396\ \mu s$ for Kr are due to acoustic waves crossing the laser axis after being reflected from the cell walls;[8,24] for Xe, the speed of sound is so slow that the reflected wave arrives at a later time. Similar acoustic features appear in the SO_2/rare gas experiments.

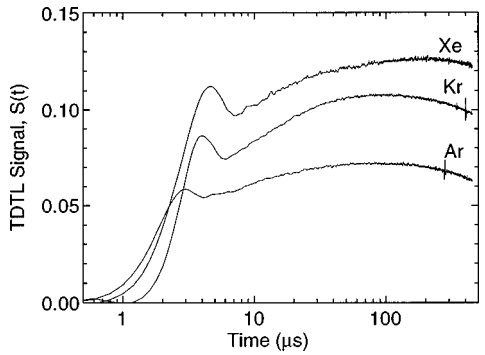

FIG. 3. TDTL signals (scaled with laser power and total pressure) obtained from dilute mixtures of CS_2 in the various bath gases at about 600 Torr pressure.

The widths of the acoustic spikes and the subsequent decay of the signal by thermal conductivity depend sensitively on the radius of the excitation laser beam, which must be determined by experiment. Once the beam radius is known, numerical simulations are used to analyze the experimental data.

1. Characterization of the pump laser beam

The TDTL theory used here assumes the use of a Gaussian beam profile, but perfect Gaussian laser beam profiles are hard to obtain in practice, especially using side-pumped dye cells. A Bethune Cell dye laser amplifier stage produced a near-circular output beam spatial profile, which was measured with a fast photodiode mounted behind a pinhole on a translation stage. Contour plots of intensity as a function of position were obtained, as shown in Fig. 4. The radial intensity distribution, $J(r)$ about the beam axis was always adequately fitted by $J(r) = J_0\ \exp[-(r/r_b)^n]$, where J_0 is a proportionality constant, n ranged from 1.65 to 2.2, and r_b ranged from 0.060 to 0.072 cm, in good agreement with values determined from the observed thermal conductivity decay (discussed below and see Tables III and IV). To test the sensitivity of the TDTL signal on the beam shape, numerical simulations were carried out for varying n values. No significant change in the thermal lens signal was observed for $n = 2.0 \pm 0.4$ and so we adopted $n = 2$ in the subsequent data analysis.

The characteristic radius, r_b of a Gaussian excitation laser beam can be determined from the long-time behavior of the TDTL signals for experimental runs at high pressure.

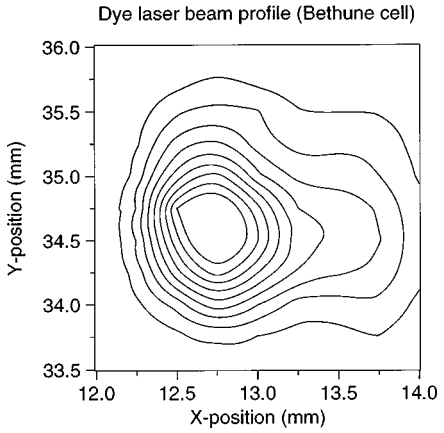

FIG. 4. A contour plot of the intensity profile of the exciting laser beam showing near-circular symmetry about the beam spot. Typically, the radial intensity distribution about the beam axis was adequately described by $J = J_0 \exp(-r/r_b)^n$, where J_0 is an arbitrary constant, n ranged from 1.65 to 2.2, and r_b, which ranged from 0.060 to 0.072 cm^{-1}.

Under these conditions, the energy transfer process is completed relatively quickly and the TDTL signal decay depends just on thermal conductivity. When thermal conductivity dominates, the intensity decays according to the following expression:[34]

$$C^{-1}\left\{\left[\frac{I}{I_0}\right]^{-1/2}-1\right\}^{-1/2}=(t+\tau_c), \tag{3}$$

where I and I_0 were defined above, C is a constant and τ_c is the time constant for dissipation of the thermal lens. The time constant, τ_c is related to r_b by the expression

$$\tau_c=\frac{PC_p r_b^2}{4RT\lambda}, \tag{4}$$

where P is the total gas pressure, C_p is the molar heat capacity at constant pressure, R is the gas law constant, T is the temperature, and λ is the thermal conductivity coefficient. For dilute mixtures of CS_2 and SO_2 in the rare gases, these parameters depend almost exclusively on the rare gas. Experimental I/I_0 data as a function of time were fitted to Eq. (3) by nonlinear least squares, as shown in Fig. 5, to obtain τ_c. The characteristic beam radius r_b, which is needed for the simulation calculations, was then obtained using Eq. (4).

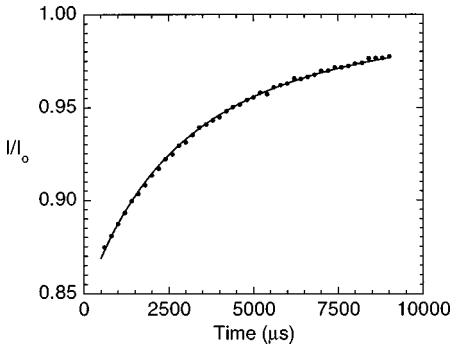

FIG. 5. Example graph of I/I_0 vs time, t for the determination of the characteristic beam size parameter, r_b. Data obtained from the long time behavior of run #12.

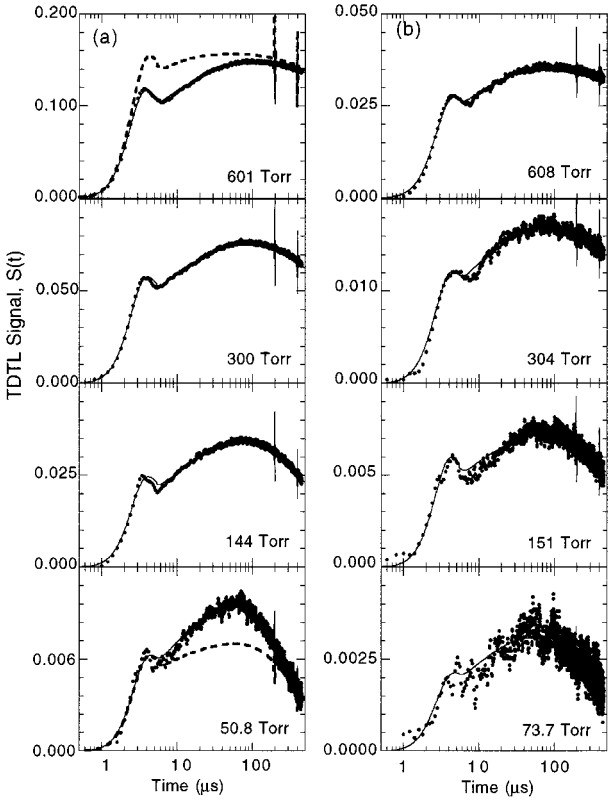

FIG. 6. Experimental and calculated TDTL signals for excited CS_2 [panel (a)] and excited SO_2 [panel (b)] in baths of Kr gas at different pressures. The corresponding experimental conditions and parameters of $V-T$ rate coefficient, k_e used to simulate each TDTL signal are listed in Tables III as runs #9–#12, and in Table IV as runs #9–#12.

2. TDTL simulations

In the TDTL experiments, the phenomenological energy transfer rate is given by[8]

$$\frac{d\langle E\rangle}{dt}=-k_e\langle E\rangle, \tag{5}$$

where $\langle E\rangle$ is the bulk average internal energy of excited species and k_e is a phenomenological rate coefficient, which is assumed to depend on $\langle E\rangle$. As $\langle E\rangle$ decays with time, the energy appears as translational energy in the bath and produces the temperature increase. The parameters and functionality of k_e were adjusted empirically to obtain agreement between simulation and experiment. The simplest form for k_e found to adequately reproduce the shape of the signals in all of the high dilution experiments is

$$k_e=A\,\exp\left(\frac{E_0-\langle E\rangle}{E_c}\right)^a+B\langle E\rangle^b, \tag{6}$$

where A, a, E_c, B, and b are empirical parameters, and E_0 is the initial excitation energy. Other empirical functions gave similar results for the energy decay, as long as the simulations accurately described the TDTL data.

B. Energy transfer results

The parameters of k_e for individual runs are listed in Tables III and IV. In Fig. 6, experimental and calculated

TDTL signals for typical experiments are shown for excited CS_2 in Kr and excited SO_2 in Kr. Simulations of similar quality were obtained for most of the experimental runs. Since the initial spike has a time constant about 2 orders of magnitude shorter than that of the final decay, a logarithmic time axis is used in the figures to aid in displaying the general quality of the simulations. The bulk of energy transfer occurs during the time period which includes the spike and shortly thereafter; the later decay of the signal is mostly due to thermal conductivity. It is evident from these plots that the simulations reproduce the major features of experimental signals with reasonable accuracy. Because of their relative molar refractivities, the signals obtained with Xe were strongest and least noisy, while those obtained with Ar were usually very weak, noisy, and difficult to simulate. Trial experiments using Ne and He produced signal strengths too weak to be useful.

The average energy $\langle E \rangle$ of the excited species at any given time was obtained by integrating Eq. (5) and using Eq. (6). The relationship between k_e, $\langle E \rangle$, and $\langle \Delta E \rangle$, the bulk average energy transferred per Lennard-Jones collision has been shown to be[8]

$$k_e = \frac{-k_{\mathrm{LJ}} \langle \Delta E \rangle}{\langle E \rangle}, \tag{7}$$

where k_{LJ} is the Lennard-Jones collision rate constant. This equation is used to derive $\langle \Delta E \rangle$ as function of $\langle E \rangle$, resulting in plots shown in Fig. 7. We also carried out simulations of the TDTL data by using empirical expressions for $\langle \Delta E \rangle$ as functions of $\langle E \rangle$ and then using Eq. (7) to obtain k_e for use in the simulations. As long as the TDTL signals were simulated accurately, the calculated decay of $\langle E \rangle$ was the same as before, showing that the choice of k_e or $\langle \Delta E \rangle$ functions in simulating the data have no effect on the final results.

The results in Fig. 7 show a marked increase in energy transfer efficiency above energies greater than $\sim 20\,000\ \mathrm{cm}^{-1}$ and a near-quadratic energy dependence of $\langle \Delta E \rangle$ at lower energies for both CS_2 and SO_2 deactivated by rare gases. The energy at which $\langle \Delta E \rangle$ changes behavior varies from run to run, due to experimental noise, but the change appears to occur over the $17\,500-23\,500\ \mathrm{cm}^{-1}$ range for CS_2/rare gas systems, and over $18\,000-22\,500\ \mathrm{cm}^{-1}$ in SO_2/rare gas systems.

Furthermore, the energy loss profiles show a systematic pressure dependence in both CS_2 and SO_2 deactivation at energies below these ''thresholds.'' Energy transfer per collision is more efficient when the collision frequency is low. In Fig. 6(a), the rate coefficients giving good simulations at 600 and at 51 Torr, respectively, were scaled appropriately and used to simulate experiments at 51 and at 600 Torr, respectively (broken curves). The broken line curves at both pressures differ in both shape and magnitude from the experiments, demonstrating that the systematic pressure dependence is significant and not due to the experimental or simulation uncertainties discussed below. To our knowledge, this effect has not been previously reported and it did not appear in the TDTL measurements[8] using NO_2. To determine whether the effect was overlooked in that study, we reanalyzed all of the NO_2 data from the earlier study and found no significant pressure dependence.

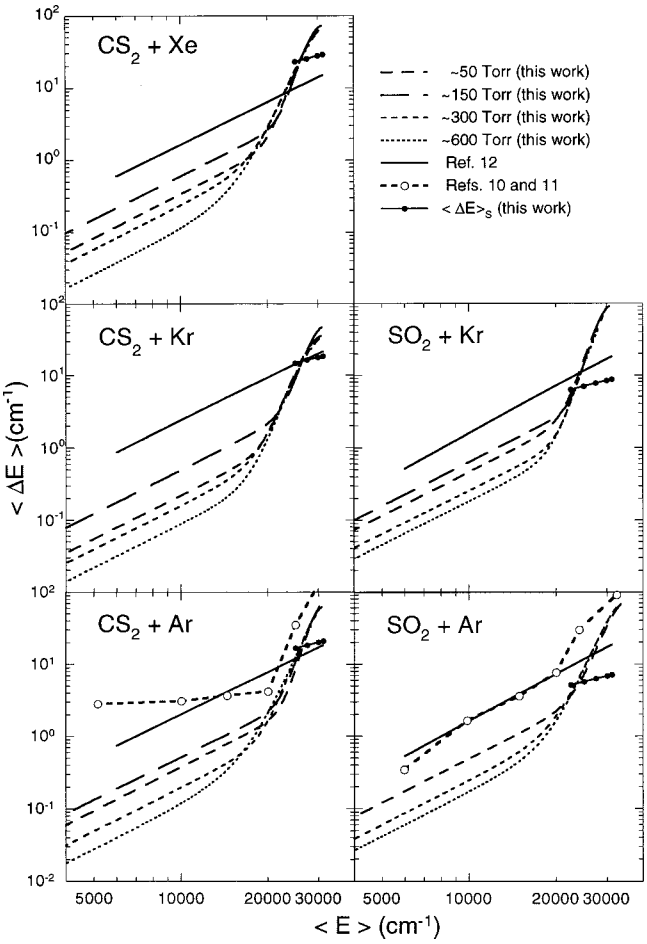

FIG. 7. The magnitude of the average energy $\langle \Delta E \rangle$ transferred per collision, as a function of $\langle E \rangle$, the mean excitation energy. Also shown are results from UVA (Ref. 10) and TR-FTIRE studies (Refs. 11 and 12). The line labeled $\langle \Delta E \rangle_s$ refers to collisional relaxation among singlet vibrational levels only [see Eq. (12)].

C. Sensitivity tests and examination of potential sources of errors

As discussed above, the signal strengths depend primarily on the total pressure, the initial concentration of excited species, laser pulse energy, and the molar refractivity of the bath gas. We estimate that the net overall experimental uncertainty (in measurements of pressure, laser power, beam radius, optical lengths) is about $\pm 25\%$. In general, the *absolute* signal strengths from simulations agreed with experiment within 30% and the deviations appear to be random. It is therefore unlikely that the unusual pressure effects observed in the experiments are the result of an unrecognized source (or sink) of heat in the system.

The shapes of the calculated TDTL signals are sensitive to the beam radius and the rate coefficient. As in the TDTL study of NO_2,[8] we found that tolerable simulations could be obtained only if r_b is within $\pm 5\%$ of the experimental value (assuming a Gaussian laser profile; see below). We also found that a 10% variation in k_e can still produce acceptable

TABLE V. Recommended fitted parameters[a] for the proposed relaxation model.

	X_T^0	a_1 ($\text{Torr}^{-1}\,\text{s}^{-1}$)	a_2 (10^{-5} s^{-1})	$10^4\times a_3$ ($1/\text{cm}^{-1}$)	a_T $\text{Torr}^{-1}\,\text{s}^{-1}/\text{cm}^{-1}$	a_S $\text{Torr}^{-1}\,\text{s}^{-1}/\text{cm}^{-1}$
CS_2/Xe	0.68	753	0.9	0.02 ± 0.18	430	25
CS_2/Kr	0.69	824	1.6	2.0 ± 4.9	217	15
CS_2/Ar	0.68	432	0.7	0.003 ± 0.33	425	18
SO_2/Kr	0.84	728	1.2	4.4 ± 0.4	135	4.8
SO_2/Ar	0.83	458	1.0	3.7 ± 0.9	46	4.1

[a]The estimated uncertainty in all fitted parameters is less than $\pm20\%$, except where indicated for a_3. X_0^T is the initial fractional population of excited molecules in the T electronic state. The initial fraction of excited molecules in the S electronic state is $X_0^S=1-X_0^T$. The energy origin are set at $E_0^T=24\,800\ \text{cm}^{-1}$ for CS_2, and $E_0^T=20\,000\ \text{cm}^{-1}$ for SO_2; see the text for details.

simulations of the 50 Torr data, but k_e is more highly constrained at higher pressures, because of the better S/N ratios.

The effect of a non-Gaussian excitation laser profile on the results was examined in two ways. As mentioned above, we carried out theoretical simulations using assumed laser beams with azimuthal symmetry, but non-Gaussian radial profiles and the energy transfer results were largely unaffected for the range of laser beam shapes observed in these experiments. We also carried out experiments in which we replaced the usual Bethune cell in the dye laser system (which gives the nearly circular spatial profile shown in Fig. 3) with an ordinary side pumped dye laser amplifier stage (which produces a strongly noncircular profile). Taking into account the change in r_b, the shape of TDTL signals and the deduced energy decay curves remained essentially the same. The insensitivity of the TDTL signal shape to the laser beam spatial profile is probably because the narrow dimension of the laser beam dominates in controlling both the acoustic waves during the initial spike and the rate of thermal conductivity dissipation of the thermal lens.

Possible computational errors were investigated by completely rewriting the TDTL computer code: the results were the same as before.

The laser excitation photon energies used here are well below the dissociation limits of CS_2 and SO_2 (see Tables I and VI) and therefore no free radical reactions are expected.

TABLE VI. Low-lying electronic states of CS_2 and SO_2.

Molecule	Dissociation limit, D_e	Electronic states below initial excitation energy
CS_2	35 997.1[a]	$^1B_2$ −30 899[b]
		$^1A_2$ −29 438[c]
		$^3A_2$ −26 187[a,d]
		$^3B_2$ −24 800[h]
SO_2	45 400[e]	$^1B_1$ −29 622[e]
		$^3B_1$, $^3A_2$, ~(24 195–27 824)[f]
		$^3B_2$ - origin around 20 000[g]

[a]Referene 29.
[b]Reference 52.
[c]Reference 54.
[d]Reference 55.
[e]Reference 30.
[f]Reference 53.
[g]Reference 11.
[h]References 37 and 38.

As mentioned earlier, the low CS_2 and SO_2 partial pressures and the low laser fluences help to minimize the possibility of reactions involving excited states and the possibility of multiphoton absorption. Experimental TDTL signals were obtained using widely differing mixing ratios and the results were practically identical for mixing ratios smaller than 1/1200. This indicates that the contribution of self-relaxation to collisional energy transfer is negligible at the 1/2500 mixing ratio employed in this study.

D. Proposed kinetics model

In our preliminary report,[14] we presented the simple kinetic relaxation model depicted in Fig. 8 for the vibrational deactivation of highly excited CS_2 in Kr bath gas. This model can be used to explain the pressure effect on energy transfer at low $\langle E\rangle$, as well as the transition to enhanced energy transfer at high $\langle E\rangle$. We assume that vibrational levels in highly excited CS_2 or SO_2 can be categorized into two sets; one set with strong singlet (ground) electronic state character, and the other with a predominance of triplet state character. This is an obvious simplification, because several excited electronic states may be involved and all may be mixed with the ground state. We label the sets as S and T states, respectively, and assume that the initial excited CS_2 or SO_2 population is distributed between the categories with fractions X_0^T and X_0^S. The model S vibrational levels have

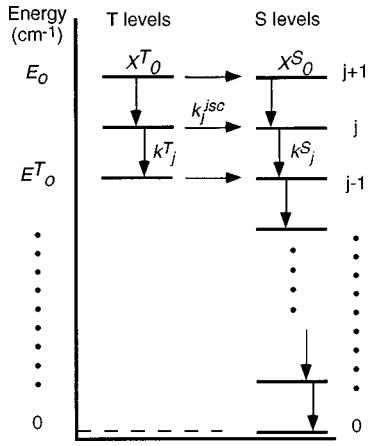

FIG. 8. Schematic representation of the model for stepwise vibrational relaxation and ISC in highly excited CS_2 and SO_2.

energy origin $E=0$, and the T origin is at $E=E_0^T$, where the energy E is the total vibronic energy. Note that $\langle E\rangle$ is the bulk average energy averaged over the entire population distribution of excited species, while E is a specific energy. The energy scale is divided into ''grains'' of nearly equal energy spacing δE; for a particular vibronic energy $E=E_j=j\ \delta E$. The fractions of species in the S and T electronic states are governed by

$$\frac{dX_j^T}{dt}=-(k_j^T+k_j^{isc})X_j^T+k_{j+1}^T X_{j+1}^T, \tag{8a}$$

$$\frac{dX_j^S}{dt}=-k_j^S X_j^S+k_{j+1}^S X_{j+1}^S+k_j^{isc}X_j^T. \tag{8b}$$

In these expressions, k_j^i is the pseudo-first-order vibrational deactivation rate coefficient, which is assumed to be proportional to the vibrational energy

$$k_j^i=a_i P_M(E_j-E_0^i), \tag{9}$$

where P_M is the pressure of the collider gas, E_0^i is the energy origin of electronic state i, and a_i in an empirical parameter. This form of k_j^i is suggested by Landau–Teller and SSH theories for energy transfer involving harmonic oscillators.[1] When the energy dependence is allowed to vary in the least squares analysis (i.e., using $k_j^i=a_i\ P_M(E_j-E_0^i)^n$, where n is fixed at values from 0 to 4), it was found that $n=1.0\pm0.1$. For simplicity in the least squares analysis, we have assumed that $n=1$ and have adopted the form of Eq. (9) in the subsequent analysis.

Collision-induced nonradiative transitions between the S and T manifolds at energy E_j is characterized by the rate coefficient k_j^{isc} which is assumed to be given by the expression

$$k_j^{isc}=\frac{a_1 P_M}{1+a_1 a_2 P_M}\exp\{a_3(E_j-E_0^T)\}, \tag{10}$$

where a_1, a_2, and a_3 are empirical parameters and P_M is the pressure of quencher. The exponential factor accounts for energy dependence, which may be important at high values of E_j. The remaining factor accounts for the mixed order kinetics, and has been adopted from collisional quenching studies[20] of the $^3B_1$ state of SO_2. The simple exponential energy dependence was chosen, because the energy dependences of the individual parameters is not known. Furthermore, the least squares analysis showed that parameter a_3 is small. At energies lower than the origin of the T state, $k_j^{isc}=0$.

Fluorescence and phosphorescence were neglected in this phenomenological model, because they are too slow to compete with the collisional processes. For simplicity, reverse processes also were neglected, but more complete models could include microscopic reversibility and detailed balance. If more detailed experimental data were available, the model could be extended to include specific vibronic states, but the TDTL experiments are not sufficiently direct to warrant such a detailed model.

In our preliminary report,[14] k_j^{isc} was represented by a linear pressure dependent term and a pressure-independent term which had an exponential energy dependence. The TDTL data are also consistent with that model (based on the goodness of least squares fits), but Eq. (10) is preferred because it is more directly related to collision-induced intersystem crossing experiments, which show saturation at higher pressures.

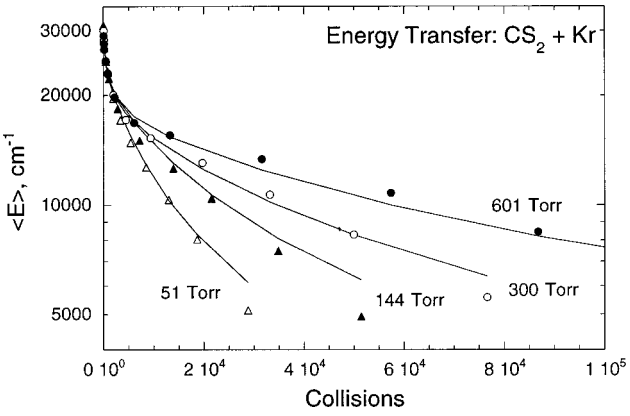

FIG. 9. Plots of CS_2 mean vibrational energy vs collisions at (a) 601 Torr, (b) 300 Torr, (c) 144 Torr, and (d) 51 Torr. Energy loss profile data (at selected energy points) are depicted as symbols and the lines show the relaxation model least squares fit. For clarity, only a representative set of pressure runs is shown.

The system of differential equations above was solved numerically using Hindmarsh's version[35] of the Gear algorithm for stiff differential equations. The fractional populations in each level were used to calculate the average internal energy, which was compared with the energy decays deduced from the TDTL experiments. The parameters for these rate coefficients and the initial relative fraction X_0^T (and $X_0^S=1-X_0^T$) were obtained by nesting the Gear–Hindmarsh numerical routine in a Levenberg–Marquardt nonlinear least squares algorithm[36] and fitting data taken from the plots of $\langle E\rangle$ vs collisions deduced from TDTL simulations. The calculated bulk average energy is given by

$$\langle E\rangle=\sum_j\ (X_j^S+X_j^T)E_j, \tag{11}$$

where the time-dependent population fractions of each level were obtained from the least-squares fit. Figures 9 and 10 illustrate such least squares fits. The triplet energy origin, E_0^T, was set at 24 800 cm^{-1} for CS_2, corresponding to the $^3B_2$ origin: the lowest triplet state, according to *ab-initio* calculations.[37,38] For SO_2, we adopted E_0^T, = 20 000 cm^{-1}, which is believed to be the origin of the lowest triplet state (also $^3B_2$).[11]

The energy grain size, δE is strongly correlated to vibrational deactivation rate parameters, a_S and a_T. The fitted parameters listed in Table V were obtained with $\delta E\approx410\ cm^{-1}$ for CS_2 and $\delta E\approx525\ cm^{-1}$ for SO_2 (these δE values are close to the bending mode energies in the respective molecules). It appears that the T state is vibrationally deactivated at a faster rate than the S state in both species, in qualitative agreement with other systems.[39,40] According to the least squares results, about 68% of the excited CS_2 and 82% of the excited SO_2 are found initially in the T state.

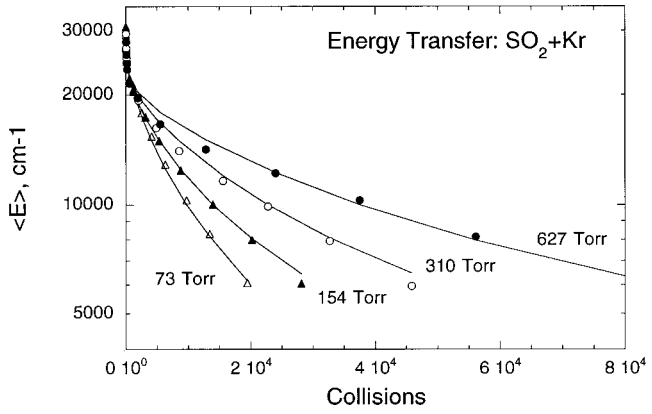

FIG. 10. Plots of SO_2 mean vibrational energy vs. collisions at (a) 627 Torr, (b) 310 Torr, (c) 154 Torr, and (d) 73 Torr. Energy loss profile data (at selected energy points) are depicted as symbols and the lines show the relaxation model least squares fit. For clarity, only a representative set of pressure runs is shown.

For each excited species, the vibrational deactivation rate coefficient shows no significant mass effect among the different colliders, in agreement with other collisional energy transfer studies.[8–11,12,13,40]

V. DISCUSSION

The model proposed here and the fitted parameters indicate that collisional deactivation in both electronic states is very rapid, but collision-induced nonradiative decay is slow. This combination produces a simple qualitative picture of the overall deactivation process. Initially, about 20%–30% of the population resides in the S state and the balance resides in the T state. After a short time period, the vibrational relaxation in both states is virtually complete, but little nonradiative decay has taken place. The energy lost by vibrational deactivation corresponds to about half of the absorbed laser energy and the short time period corresponds to the rapid deactivation prior to the characteristic elbow in the TDTL data. At this point, the remaining excited population resides in the triplet state and has little vibrational energy. Subsequent deactivation proceeds via slow CIISC decay. At bulk average energies below the elbow, the deactivation corresponds to the CIISC rate and *does not depend on vibrational relaxation*. If the CIISC decay was rapid and did not constitute the rate limiting step, no elbow would be apparent in the TDTL data. The memory effect arises because the slow CIISC decay rate shows the typical linear pressure dependence at low pressures, and a pressure saturation at high pressures; our experimental pressure range lies in the intermediate ''turnover'' region.

In this model, the parameter a_1 represents the collisional quenching rate, and $a_2^{-1}\exp\{a_3(E_j-E_0^T)\}$ is the pressure-independent limiting rate of the T manifold of SO_2 (or CS_2) with its origin set at the $^3B_2$ energy origin. For SO_2, the values of a_3 appear to indicate similar energy dependences of k_j^{isc} for Ar and Kr, whereas for CS_2, the uncertainty in a_3 for the three collider gases is so large that a significant trend cannot be discerned. In all cases, the values obtained for the parameter a_3 suggest that the energy dependence of k_j^{isc} is not large enough to play a significant role over the limited energy range above E_0^T, in the present experiments. When the T manifold origin was set at the energy origin of the lowest triplet states that have been directly observed ($^3B_1$ in SO_2 and $^3A_2$ in CS_2), the energy transfer data either would not fit the model or resulted in poorer least squares fits. In the previous studies on the $^3B_1$ in SO_2 by Strickler and Rudolph,[20] the collision quenching rate, k_q, with N_2 as the quenching gas, was found to be about 4.6×10^3 $Torr^{-1}\,s^{-1}$. The limiting (pressure independent) rate, $1/\alpha$ was found to be 1.3×10^6 s^{-1}. The corresponding rates from our model are about an order of magnitude slower, perhaps because they refer to a different electronic state ($^3B_2$) in the T manifold. If rapid internal conversion takes place from the $^3B_1$ state to the lower $^3B_2$ state, followed by slow, rate-limiting CIISC from the $^3B_2$, then the result is consistent with the TDTL experiments. Energy transfer in the reverse direction is effectively inhibited as long as the $^3B_2$ state is several kT lower in energy than the $^3B_1$ state. No further comparisons can be made since there are no lifetime measurements or calculations of the $^3B_2$ state in either SO_2 or CS_2.

The marked increase in energy transfer (the ''elbow'') at energies near and above the origin of low lying electronic states was noted first in a TDTL study of NO_2 relaxation[8] and it has also been reported in TR-FTIRE measurements involving highly excited NO_2,[9,10(b)] CS_2,[10(a)] and SO_2.[11] In the TR-FTIRE studies of SO_2,[11] for example, total pressures ranged from 100 to 300 Torr and the SO_2/Ar mixing ratio was 1/300, necessitating corrections for SO_2–SO_2 self-quenching. After subtraction of the self quenching, $\langle\Delta E\rangle$ was of the order of $1\,cm^{-1}$ (see Fig. 7) and no pressure variations were noted.[41] Hartland *et al.*[10(a)] have argued that the enhanced V–V energy transfer observed for nonmonatomic colliders above the energy elbow is due to vibronic (and, in some cases, spin–orbit) coupling of excited electronic states to the ground electronic state, which permits the electronic transition dipole to contribute significantly to the dipole–dipole energy transfer probability (this mechanism was described earlier by Chou and Flynn[56]). Recently, Hartland *et al.* have extended this argument and assert that ''vibronic couplings will enhance $V-T$, R energy transfer if an optical transition between the coupled states is allowed,'' due to changes in the long range interactions.[10(b)] Although their model has yet to be verified and the magnitude of the effect in these systems ascertained, such a mechanism may help to explain why a_T is so much larger than a_S (Table V). However, their models taken alone cannot explain the pressure saturation effect observed in the present experiments. Furthermore, they do not explain why the UVA experiments did not find an elbow.

The UVA studies of CS_2[12] and SO_2[13] detected neither the elbow, nor the pressure dependence, but found a near-quadratic energy dependence of $\langle\Delta E\rangle$ throughout the energy range. In Fig. 7, values of $\langle\Delta E\rangle$ obtained in the present work are compared with those from other studies. It has been surmised[10(a)] that the UVA studies did not detect the elbow, because of problems associated with calibrating the optical extinction coefficient against excitation energy. However, within the context of the model proposed in the present

work, the UVA technique would not have observed the elbow, because the absorption it is sensitive only to the ground (singlet) state population and therefore the definition of both $\langle E \rangle$ and $\langle \Delta E \rangle$ in the UVA experiments differs from those used here. The present results can be compared with the UVA experiments by considering k_j^S at the high energies where the TDTL results depend on it most strongly. The corresponding values of $\langle \Delta E \rangle_s$ for vibrational deactivation of the S state can be estimated from the expression

$$\langle \Delta E \rangle_s = \delta E k_j^S / k_{\mathrm{LJ}}. \tag{12}$$

As shown in Fig. 7, the values of $\langle \Delta E \rangle_s$ agree reasonably well with the UVA results at the high energies.

In the TR-FTIRE studies,[9–11] the energy is deduced by measuring the anharmonic shift and broadening of infrared emission spectral peaks and using spectral simulation coupled with a least-squares method to deduce $\langle E \rangle$ and $\langle \Delta E \rangle$. According to the present model, initially about 20%–30% of the excited molecules are in the S manifold and have high vibrational excitation, while the remainder are in the T manifold and have low vibrational excitation. The highly vibrationally excited species emit more brightly than the others and thus the emission spectrum would be dominated by the molecules in the S manifold. Once both manifolds have been vibrationally deactivated, the slow nonradiative decay will continue to supply vibrationally excited S state species at a rate depending on the decaying T state population. Thus, after the elbow, one would expect the emission spectrum to be an average of the cascading singlet state molecules and the spectral distribution would not change significantly, but its amplitude would decay with time. If some residual vibrational excitation remained in the triplet state, the spectral distribution would be due to vibrational emission from both singlet and triplet state molecules in gradually varying proportions, and the spectral shifts would vary gradually with time as the amplitude decayed. Since the spectral simulations used in analyzing the TR-FTIRE experiments are not perfect (there are even some unassigned spectral features) and energy randomization among all states within arbitrary energy grains is specifically assumed (despite the sparse densities of states), there is some latitude for alternative interpretations: It would be interesting to re-examine the TR-FTIRE data from the perspective of the present model.

It should be noted that although the kinetic model presented here is plausible and it explains the TDTL data and most of the previous results, it is highly simplified and needs to be confirmed by more direct techniques in future studies. Regardless of whether this proposed kinetics model is confirmed, the energy transfer data (including the unusual pressure effect) extracted from the TDTL signals appear to be robust. Potential artifacts and experimental errors have been investigated and none has been found which can significantly affect the energy decays. Ultimately, direct experiments on the excited electronic states are needed to determine whether the proposed model is the correct explanation for the TDTL data.

VI. SUMMARY

Our results indicate that the energy transferred per collision depends on the vibrational energy content of CS_2 and, on the collision frequency. At all collision frequencies, $\langle \Delta E \rangle$ is large and strongly energy dependent at high energies. At energies below about 20 000 cm^{-1}, the energy dependence of $\langle \Delta E \rangle$ is weaker and dominated by a slow nonradiative process. For both CS_2 and SO_2, a sharp turn in energy dependence (from near-quadratic at low energies to a stronger dependence at high energies) occurs, due to a bottleneck in the energy transfer among excited electronic states. A simplified phenomenological model which includes collisional vibrational relaxation within each of two sets of electronic state, and a collision-induced nonradiative decay rate exhibiting mixed order kinetics has been used to explain both the enhanced energy transfer at high energies and the memory effect observed here. The memory effect appears to be an important feature of energy transfer, especially for small molecules where a collision-induced nonradiative transition from a low lying electronic state proceeds at a rate comparable to or slower than vibrational relaxation.

ACKNOWLEDGMENTS

This work was funded, in part, by the U.S. Department of Energy, Office of Basic Energy Sciences. We thank Irio Calasso, David S. Perry and George W. Flynn for stimulating discussions, and Hai-Lung Dai for helpful comments and for communicating results prior to publication.

[1] (a) J. D. Lambert, *Vibrational and Rotational Relaxation in Gases* (Clarendon, Oxford, 1977); (b) R. N. Schwartz, Z. I. Slawsky, and K. F. Herzfeld, J. Chem. Phys. **20**, 5091 (1952); (c) R. N. Schwartz and K. F. Herzfeld, *ibid.* **22**, 767 (1954); (d) F. I. Tanczos, *ibid.* **25**, 439 (1956); (e) J. T. Yardley, *Introduction to Molecular Energy Transfer* (Academic, New York, 1980).
[2] B. J. Orr and I. W. M. Smith, J. Phys. Chem. **91**, 6106 (1987).
[3] B. J. Orr, Adv. Chem. Kin. Dyn. **2A**, 21 (1995).
[4] D. C. Clary, J. Phys. Chem. **91**, 1718 (1987).
[5] D. C. Clary and G. J. Kroes, Adv. Chem. Kin. Dyn. **2A**, 135 (1995).
[6] H. Hippler and J. Troe, in *Bimolecular Collisions*, edited by J. E. Baggott and M. N. Ashfold (The Royal Society of Chemistry, London, 1989), 209.
[7] I. Oref and D. C. Tardy, Chem. Rev. **90**, 1407 (1990).
[8] B. M. Toselli, T. L. Walunas, and J. R. Barker, J. Chem. Phys. **92**, 4793 (1990).
[9] G. V. Hartland, D. Qin, and H.-L. Dai, J. Chem. Phys. **100**, 7832 (1994).
[10] (a) G. V. Hartland, D. Qin, and H.-L. Dai, J. Chem. Phys. **102**, 8677 (1995); (b) G. V. Hartland, D. Qin, H.-L. Dai, and C. Chen, *ibid.* **107**, 2890 (1997).
[11] D. Qin, G. V. Hartland, H.-L. Dai, and C. L. Chen, J. Phys. Chem. (to be published).
[12] J. E. Dove, H. Hippler, and J. Troe, J. Chem. Phys. **82**, 1907 (1985).
[13] M. Heymann, H. Hippler, D. Nahr, H. J. Plach, and J. Troe, J. Phys. Chem. **92**, 5507 (1988).
[14] A. Chimbayo, B. M. Toselli, and J. R. Barker, Chem. Phys. Lett. **259**, 225 (1996).
[15] H. S. Johnston, C. E. Miller, B. Y. Oh, K. O. Patten, Jr., and W. N. Sisk, J. Phys. Chem. **97**, 9890 (1993).
[16] K. O. Patten, Jr. and H. S. Johnston, J. Phys. Chem. **97**, 9904 (1993).
[17] W. N. Sisk, C. E. Miller, and H. S. Johnston, J. Phys. Chem. **97**, 9916 (1993).
[18] J. J. F. McAndrew, J. M. Preses, R. E. Weston, and G. W. Flynn, J. Chem. Phys. **90**, 4772 (1989).
[19] A. E. Douglas, J. Chem. Phys. **45**, 1007 (1966).
[20] (a) R. N. Rudolph and S. J. Strickler, J. Am. Chem. Soc. **99**, 3871 (1977); (b) S. J. Strickler and R. N. Rudolph, *ibid.* **100**, 3326 (1978); (c) S. J. Strickler and R. D. Ito, J. Phys. Chem. **89**, 2366 (1985).

[21] F. Su, F. B. Wampler, J. W. Bottenheim, D. L. Thorsell, J. G. Calvert, and E. K. Damon, Chem. Phys. Lett. **51**, 150 (1977).
[22] K. F. Freed, J. Chem. Phys. **64**, 1604 (1976).
[23] K. F. Freed, Adv. Chem. Phys. **47**, 291 (1981).
[24] J. R. Barker and B. M. Toselli, *Photothermal Investigations of Solids and Fluids*, edited by J. A. Sell (Academic, New York, 1989), Chap. V.
[25] P. L. Trevor, T. Rothem, and J. R. Barker, Chem. Phys. **68**, 341 (1982).
[26] H. Sontag, A. C. Tam, and P. Hess, J. Chem. Phys. **86**, 3950 (1987).
[27] S. P. Sapers and D. J. Donaldson, J. Phys. Chem. **91**, 8918 (1990).
[28] J. L. Hardwick, Y. Ono, and J. T. Moseley, J. Phys. Chem. **91**, 4566 (1987).
[29] *JANAF Thermochemical Tables*, 3rd ed. J. Phys. Chem. Ref. Data Suppl. **14**, No. 1 (1985).
[30] C. S. Effenhauser, P. Felder, and J. R. Huber, Chem. Phys. **142**, 311 (1990).
[31] J. R. Barker and T. Rothem, Chem. Phys. **68**, 331 (1982).
[32] S. J. Jacobs, Chem. Phys. **132**, 71 (1989).
[33] (a) D. R. Siebert, F. R. Grabiner, and G. W. Flynn, J. Chem. Phys. **60**, 1564 (1974); (b) D. R. Siebert, F. R. Grabiner, and G. W. Flynn, *ibid.* **17**, 189 (1974); (c) D. R. Siebert, Ph.D. thesis, Columbia University, 1973; (d) F. R. Grabiner, Ph.D. thesis, Columbia University 1974.
[34] R. T. Bailey, F. R. Cruickshank, R. Guthrie, D. Pugh, and I. J. M. Weir, Chem. Phys. **114**, 411 (1987).
[35] A. C. Hindmarsh, *Scientific Computing*, edited by R. S. Stepleman *et al.* (North-Holland, Amsterdam, 1983) pp. 55–64.
[36] P. R. Bevington, *Data Reduction and Error Analysis for the Physical Sciences* (McGraw-Hill, New York, 1969), Chap. 11.
[37] Q. Zhang and P. H. Vaccaro, J. Phys. Chem. **99**, 1799 (1995).
[38] D. C. Tseng and R. D. Poshusta, J. Chem. Phys. **100**, 7481 (1994).
[39] T. J. Bevlacqua and R. B. Weisman, J. Chem. Phys. **98**, 6316 (1992).
[40] L. A. Miller and J. R. Barker, J. Chem. Phys. **105**, 1383 (1996).
[41] H.-L. Dai (private communication, 1997).
[42] C. H. Hearn and J. A. Joens, J. Quant. Spectrosc. Radiat. Transf. **45**, 69 (1991).
[43] R. C. Reid, Prausnitz and T. K. Sherwood, *The Properties of Gases and Liquids* (McGraw-Hill, New York, 1966).
[44] F. M. Mourits and F. H. A. Rummens, Can. J. Chem. **55**, 3007 (1977).
[45] J. Troe, J. Chem. Phys. **66**, 4758 (1977).
[46] M. Born and E. Wolf, *Principles of Optics* (Pergamon, New York, 1975), p. 88.
[47] C. E. Hecht, *Statistical Thermodynamics and Kinetic Theory* (Freeman, New York, 1990).
[48] E. A. Moelwyn-Hughes, *Physical Chemistry* (Pergamon, New York, 1961), p. 383.
[49] *CRC Handbook of Chemistry and Physics*, 66th ed. (CRC, Boca Raton, 1985).
[50] C. L. Yaws, *Physical Properties* (McGraw-Hill, New York, 1978).
[51] R. T. Bailey, F. R. Cruickshank, R. Guthrie, D. Pugh, and I. J. M. Weir, Mol. Phys. **48**, 81 (1983).
[52] H. T. Liou, H. Yang, N. C. Wang, and R. W. Joy, Chem. Phys. Lett. **178**, 80 (1991).
[53] I. H. Hiller and V. R. Sanders, Mol. Phys. **22**, 193 (1971).
[54] Ch. Jungen, D. N. Malm, and A. J. Merer, Chem. Phys. Lett. **80**, 302 (1972).
[55] B. Kleman, Can. J. Phys. **41**, 2034 (1963).
[56] J. Z. Chou and G. W. Flynn, J. Chem. Phys. **93**, 6099 (1990).